Interaction-driven fractional quantum Hall state of hard-core bosons on kagome lattice at one-third filling

W. Zhu, S. S. Gong, and D. N. Sheng

Interaction-driven fractional quantum Hall state of hard-core bosons on kagome lattice at one-third filling

W. Zhu[1], S. S. Gong[2] and D. N. Sheng[1]

[1]*Department of Physics and Astronomy, California State University, Northridge, California 91330, USA and*
[2]*National High Magnetic Field Laboratory, Florida State University, Tallahassee, Florida 32310, USA*

There has been a growing interest in realizing topologically nontrivial states of matter in band insulators, where a quantum Hall effect can appear as an intrinsic property of the band structure. While the on-going progress is under way with a number of directions, the possibility of realizing novel interaction-generated topological phases, without the requirement of a nontrivial invariant encoded in single-particle wavefunction or band structure, can significantly extend the class of topological materials and is thus of great importance. Here, we show an interaction-driven topological phase emerging in an extended Bose-Hubbard model on kagome lattice, where the non-interacting band structure is topological trivial with zero Berry curvature in the Brillouin zone. By means of an unbiased state-of-the-art density-matrix renormalization group technique, we identify that the groundstate in a broad parameter region is equivalent to a bosonic fractional quantum Hall Laughlin state, based on the characterization of universal properties including groundstate degeneracy, edge excitations and anyonic quasiparticle statistics. Our work paves a way of finding interaction induced topological phase at the phase boundary of conventionally ordered solid phases.

I. INTRODUCTION

While fundamental particles in nature are either bosons or fermions, the emergent excitations in two-dimensional strongly-correlated systems may obey fractional or anyonic statistics[1,2]. The most famous example is the quasiparticles or quasiholes in fractional quantum Hall (FQH) effects in strong magnetic field, which are topological states of matter whose low-energy physics is governed by the Chern-Simon gauge theory. Interestingly, recent theoretical discoveries have revealed that FQH effects can also be realized in lattice systems in the absence of an external magnetic field[3–7]. Such a lattice realization of FQH phases is attributed to two key points: 1) a nearly dispersionless single-particle energy band with non-trivial topology characterized by a nonzero Chern number, 2) and a strong many-body interaction comparing to the band width. The condition of nearly flat topological band is essentially important, as the kinetic energy of particles can be quenched in such a topological band akin to the Landau level physics. The strong interaction also plays the vital role in stabilizing the FQH phases. In fact, without the interaction or interaction being a subleading correction, the system is expected to be in a Fermi liquid like state at fractional fillings rather than forming a topological phase.

Given above facts, a natural question that we address in this paper is whether a FQH phase is also possible in a lattice model with trivial non-interacting band. Actually, there have been a series of proposals along this direction[8–13], where the common wisdom is that the presence of strong interactions in a strongly frustrated system can give rise to a nonlocal complex bond order parameter and a spontaneous breaking of time-reversal symmetry (TRS) through flux attachment[8]. However, lacking of a theoretical method to predict the quantum phase for microscopic interacting systems, theoretical studies usually resort to different mean-field approximations, which often favor topological phases. As an example, Raghu *et. al*[10] showed that a quantum anomalous Hall effect can be dynamically generated in an extended Hubbard model on the honeycomb lattice. The similar idea has been applied to other lattice systems with a quadratic band crossing point, such as kagome[11], checkerboard[12], diamond[13] and Lieb lattice[14,15]. However, comprehensive numerical studies have been searching for true groundstates in different lattice systems and failed to find exotic topological phases predicted by the mean-field theories[16–21]. Here a crucial difficulty is that, instead of triggering the desired TRS spontaneously breaking, the strong interactions also tend to stabilize competing solid orders by breaking translational symmetry. Thus, the simple concept of realizing interaction-induced FQH phases in topological trivial bands was illusive in realistic lattice models.

Very recently, theoretical studies of extended kagome anti-ferromagnetic systems have discovered a particular class of spin liquids, the so-called chiral spin liquid[22,23], with TRS spontaneously[24,25] (or explicitly[26]) broken, which shed lights on this elusive area: Long-ranged frustrated interactions may favor the FQH-like ground state near the boundary between ordered states[27]. So far the existing examples are rare and all occur at the half-filling (half of spins are pointing up in z-direction) on kagome lattice, which may be attributed to quantum fluctuations near the non-coplanar spin ordered state (cuboc phase)[27–29]. Thus it is highly desired to search for the interaction-induced FQH phase beyond the half-filling, which serves as the proof of the principle that TRS broken phase can emerge in more general conditions without a nearby cuboc phase. On the other hand, kagome-based magnetic systems have been widely studied under an external magnetic field[61], which can tune the spin systems into different magnetizations corresponding to hardcore boson systems at different fillings. The interesting candidate states have been established including the valence bond crystal state[30–32] and the featureless Mott insulator[33] as possible groundstates. Beside these topological trivial phases, a Z_2 topological phase may survive in an easy-axis kagome system[34], which is currently under debate[35]. It is theoretically proposed that FQH state can also emerge at 1/3 filling[36,37], however, so far this possibility has not been established by controlled theoretical methods beyond mean-field approaches. Along this line, the existence of a topological

ordered phase at one-third filling remains open.

In this paper, we study an Bose-Hubbard model on the kagome lattice in the hard-core limit:

$$H = \quad t \sum_{\langle \mathbf{rr'} \rangle} \left[b_{\mathbf{r'}}^{\dagger} b_{\mathbf{r}} + \text{H.c.} \right] + V_1 \sum_{\langle \mathbf{rr'} \rangle} n_{\mathbf{r}} n_{\mathbf{r'}}$$
$$+ \quad V_2 \sum_{\langle\langle \mathbf{rr'} \rangle\rangle} n_{\mathbf{r}} n_{\mathbf{r'}} + V_3 \sum_{\langle\langle\langle \mathbf{rr'} \rangle\rangle\rangle} n_{\mathbf{r}} n_{\mathbf{r'}} \qquad (1)$$

, where $b_{\mathbf{r}}^{\dagger}$ ($b_{\mathbf{r}}$) creates (annihilates) a hard-core boson at site $\mathbf{r}$. $t = 1$ is the nearest-neighbor hopping amplitude, V_1, V_2, V_3 are the density-density repulsion strengths on first, second and third nearest neighbors, respectively. We focus on the boson filling number $1/3$ in this paper. This model can also be mapped onto the spin$-1/2$ XXZ model, allowing for an interpretation of our results in terms of both bosons and quantum spins. The energy band for hosting hardcore bosons is topological trivial (with real hopping terms) with zero Berry curvature in the Brillouin zone. In order to study the ground state phase diagram in the $\{V_1, V_2, V_3\}$ parameter space, we implement the density-matrix renormalization group (DMRG) algorithm on cylinder geometry combined with the exact diagonalization (ED) on torus geometry (see Appendix A for computational details), both of which have been proven to be powerful and complementary tools for studying realistic models containing arbitrary strong and frustrated interactions.

II. RESULTS

A. Phase Diagram

Our main findings are summarized in the phase diagram Fig. 1(a-b). In the parameter region $V_2 \approx V_3$ and $V_2, V_3 > V_1$ ($0 \leqslant V_1 \leqslant 2.0$), we find a robust FQH phase emerging with the TRS spontaneously breaking. The FQH phase is centered around the line $V_2 \approx V_3$, which persists to $|V_2 - V_3| < 0.1$ approximately as shown for $V_1 = 0$ in Fig. 1(b). The FQH phase is characterized by a four-fold groundstate degeneracy on torus geometry, which arises from two sets of Laughlin $\nu = 1/2$ FQH states with opposite chiralities. In particular, the TRS spontaneous breaking can be inspected by identifying local circulating currents on the cylinder geometry, while the nature of bosonic Laughlin $\nu = 1/2$ state will be identified by the edge excitation spectrum, fractional Chern number and the anyonic quasiparticle statistics as elaborated later. Interestingly, we also show that the FQH liquid phase is neighboring with several solid phases which all respect TRS (without emergent spin current): a strip phase, a charge density wave $q = (0,0)$ phase, and $q = (0,\pi)$ phase with q as the ordering wave vectors. Compared to the distinctive Bragg peaks in the structure factor for solid phases (Fig. 1(c-d)), the FQH phase shows a structureless feature (Fig. 1(e)). Finally, between the FQH phase and $q = (0,0)$ phase, there exists a narrow window for the coexistence of both FQH and charge density order (labeled by shaded area in Fig. 1(a)). By comparing our quantum phase diagram with the classical phase diagram, we find that the FQH phase is present near the classical phase
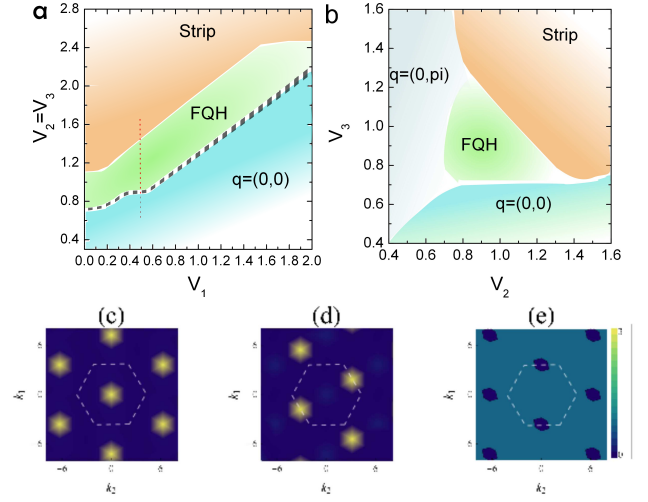

FIG. 1: Phase diagram of the extended Bose-Hubbard model on kagome lattice obtained by DMRG calculations on cylinder of circumference $L_y = 4$. (a)The phase diagram plotted in V_1 and $V_2 = V_3$ parameter space. The shaded area is a coexistence region. (b)The phase diagram plotted in V_2 and V_3 parameter space by setting $V_1 = 0$. The contour plots of static density structure factor for: (c) charge density wave $q = (0,0)$ phase, (d) strip phase and (e) FQH phase. The white dashed line shows the first Brillouin zone.

boundary neighboring with different solid phases (Appendix B). The current work provides an example of bosonic topological phase (or chiral spin liquid in spin language) beyond half-filling on kagome lattice, which distinguishes our work from earlier results at half-filling[24–26].

B. Energy Spectrum and Doubled Topological Degeneracy

Topological ordered states have characteristic groundstate degeneracy on compactified space (i.e. torus) while TRS spontaneous breaking topological phase has doubled topological degeneracy. To demonstrate this property in the intermediate FQH region, we first investigate the low-energy spectra based on ED calculation. In Fig. 2, we show the scan of energy spectra along the line $V_1 = 0.5$ and varying $V_2 (= V_3)$. It is clear shown that there is a fourfold groundstate degeneracy in the regime $0.8 < V_2 = V_3 < 1.5$, which is separated by higher excited states by a robust spectrum gap. The fourfold degeneracy arises from two-fold topological degeneracy for the $\nu = 1/2$ Laughlin state (full evidences will be shown below) and an additional factor of 2 from two-copies of states with the opposite chirality due to the TRS spontaneously breaking. All four groundstates are located in momentum sector $k = (0,0)$, consistent with the expectation of the momentum folding rule for emerging FQH state with 12 particles on $3 \times 3 \times 4$ kagome lattice[6,7]. The low-energy spectrum gap for different system sizes is shown in Fig. 2(b), where we find that the energy gap between the fourth lowest energy state and the fifth one is robust against the increase of system sizes (Fig. 2(b)). This result indicates the emergent
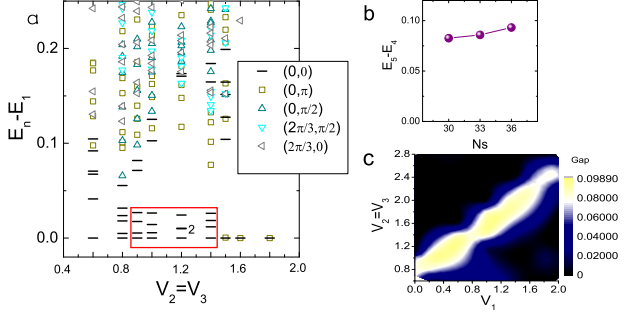
FIG. 2: Energy spectra from ED calculation. (a) A scan across the reference line in Fig. 1 by setting $V_1 = 0.5$ on the $N_s = 3 \times 3 \times 4 = 36$ sites cluster. The four-fold degeneracy of the FQH state is present around $0.8 < V_2 = V_3 < 1.5$. Different colors and symbols correspond to different momentum sectors. (b) Energy gap for various system sizes N_s by setting $V_1 = 0.5, V_2 = V_3 = 1.2$. (c)Contour plot of energy gap versus V_1 and $V_2 = V_3$ on $N_s = 36$ sites cluster.

FQH phase may be robust at thermodynamic limit, which will be further confirmed by our larger system results based on DMRG. We also find that the energy gap is robust in the whole FQH regime while it drops to near zero at the phase boundary as illustrated in Fig. 2(c).
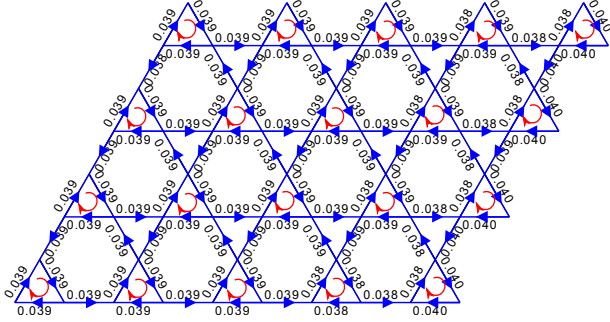

FIG. 3: Local current $\mathcal{J}_{ij}$ pattern of $|\Psi_{\mathbb{1}}^L\rangle$ from DMRG calculation. The parameter is $V_1 = 0.5, V_2 = V_3 = 1.2$ on $L_y = 4$ cylinder (only show the five columns in the center). Width of bond is proportional to the current value ($\mathcal{J}_{ij}$ is shown on the bond as a number) and arrows correspond to current directions.

C. Time Reversal Symmetry Spontaneously Broken and Local Current

Since the Hamiltonian (Eq. 1) preserves TRS, the emergent FQH state as the groundstate breaks TRS *spontaneously*. To investigate this mechanism, we move to larger systems with the cylinder geometry and obtain the groundstates $|\Psi_{\mathbb{1},s}^{L(R)}\rangle$ by implementing DMRG calculation. By using different random initial wavefunction in DMRG, we obtain four different groundstates. Here we label topologically different groundstates by their chiral and anyonic nature on cylinder geometry, where L (R) stands for "left-hand" ("right-hand") chiral-

ity, and $\mathbb{1}$ (s) stands for identity (semion) quasiparticle (see below).) A simple picture of the TRS broken can be obtained by measuring the local circulating currents in real-space. As shown in Fig. 3, the current $\mathcal{J}_{ij} = Im\langle\Psi_{\mathbb{1}}^L|b_i^\dagger b_j|\Psi_{\mathbb{1}}^L\rangle$ between two nearest-neighbor sites (i, j) forms loop structure and is in the clockwise direction in each triangle in the bulk of the system, which is referred as "left-hand" chirality. The emergent loop current is a direct demonstration of TRS spontaneously breaking for the state, which enables experimental detecting from local current measurements. Here the spin current at one-third filling is distinct from the previously discovered chiral spin liquid at half filling where the net spin current is zero[24–26]. In addition, we also find that the TRS partner $|\Psi_{\mathbb{1},s}^R\rangle$ hosts anti-clockwise loop current in each triangle.

D. Fractionalization and Fractional Statistics for Quasiparticles

To uncover the anyonic nature of groundstates in the intermediate region, we investigate hallmark signatures of FQH state including characteristic excitation spectrum on the edge, fractional Chern number and quasiparticle braiding statistics in the bulk. All the evidences we obtain fully support the topological phase in the intermediate region is the emerging bosonic $\nu = 1/2$ Laughlin state.

1. Entanglement Spectrum

Firstly, we study the characteristic edge excitation with the help of entanglement spectrum (ES)[38], as partitioning a cylinder into two halves manifests a "spatial" boundary. Fig. 4 shows the ES for two of the groundstates $|\Psi_{\mathbb{1},s}^L\rangle$ with "left" chirality. The ES is grouped by the relative boson number ΔN_L of the half system and their relative momentum quantum number ΔK_y (relative to the total K_y of the highest weight spectrum level) along the transverse direction (referred to as y-direction). The leading ES of $|\Psi_{\mathbb{1},s}^L\rangle$ displays the sequence of degeneracy pattern $\{1, 1, 2, 3, 5, ...\}$ in each ΔN_L sector. The finite splitting among degeneracy group is due to the finite size effect. Importantly, the edge mode counting rule agrees with the prediction of the free chiral boson in $SU(2)_1$ conformal field theory which describes the edge theory of Laughlin state[39]. In addition, Fig. 4 also signals the chiral nature of the edge spectrum (ES increases as K_y varies from 0 to -2π by a step $\Delta K_y = -2\pi/L_y$), which results from the TRS spontaneously breaking. The other two groundstates $|\Psi_{\mathbb{1},s}^R\rangle$ with "right" chirality have opposite chirality ($\delta K_y = 2\pi/L_y$) but the same degeneracy pattern in ES (not shown). Compared with previously works at half-filling[24–26], we did not observe the emergent $SU(2)$ symmetry between different N_L sectors, since the $\Delta N_L = 1$ is no longer equivalent to $\Delta N_L = -1$ away from half filling.
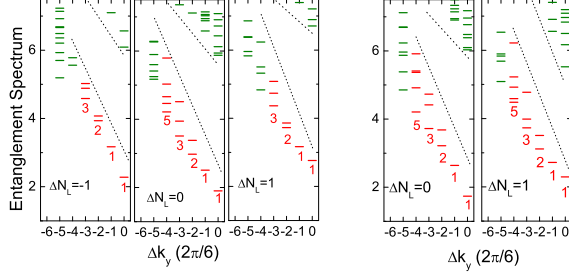
FIG. 4: The low-lying ES of $|\Psi_{\mathbb{1}}^L\rangle$ (left) and $|\Psi_s^L\rangle$ (right) on $L_y = 6$ cylinder. The ES is labeled by the relative boson number $\Delta N_L = N_L - N_L^0$ of left half cylinder in each tower (N_L^0 is the boson number of the state of reduced density matrix with the largest eigenvalue). In each tower, the horizontal axis shows the relative momentum $\Delta K_y = K_y - K_y^0$ in the transverse direction of the corresponding eigenvectors (K_y^0 is momentum of the state with the largest eigenvalue in each tower). The numbers below the red dots label the nearly degenerating pattern for the low-lying ES with different ΔK_y. The black dashed line shows the entanglement gap in each momentum sector.

2. Fractional Charge and Chern Number Quantization

Secondly, we perform a numerical flux insertion simulation on cylinder systems[24,40–42], to determine the quantization of Hall transport and the topological Chern number of the ground state. This simulation realizes Laughlin gedanken experiment[43–45], where a quantized charge will be pumped from one edge to the other edge by inserting a $U(1)$ charge flux in the hole of the cylinder for a quantum Hall state. As shown in Fig. 5 (a), by threading a flux quantum $\theta = 2\pi$, $|\Psi_{\mathbb{1}}^L\rangle$ adiabatically evolves into $|\Psi_s^L\rangle$. Further increasing flux up to 4π will drive the system back to the $|\Psi_{\mathbb{1}}^L\rangle$. Interestingly, comparing the ES at $\theta = 0$ and 4π, the adiabatic flux insertion shifts the lowest level of ES from $\Delta N_L = 0$ to $\Delta N_L = -1$, signaling a net charge transfer $\Delta Q = 1$ (a unit charge) from the left edge to the right edge. In Fig. 5(b), the net charge transfer ΔQ is demonstrated, which is nearly quantized at $\Delta Q \approx 0.50$ at $\theta = 2\pi$. Based on these observations, we identify the bulk Chern number of the groundstate as $C_{\mathbb{1}} = C_s = 1/2$, fully characterizing the obtained state as the Laughlin $\nu = 1/2$ state.

Here we identify each groundstate hosts a fractional Chern number $C = 1/2$, which is similar to the Laughlin $\nu = 1/2$ state in fractional Chern insulator[46]. The key difference is, the ground state in the fractional Chern insulator inherits the nontrivial topology from the non-interacting band. However, our extended Bose-Hubbard model (Eq. 1) has a Chern number $C = 0$ for the single-particle band. Thus, our model realizes an interaction-driven topological phase from a topologically trivial band structure[47] resulting from the spontaneous TRS breaking.
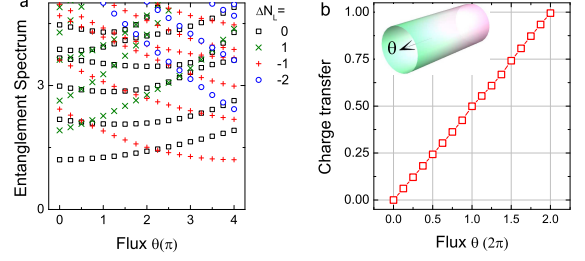

FIG. 5: (a) The ES flow with inserting flux θ in the hole of the cylinder with $L_y = 4$. Starting from the identity ground state $|\Psi_{\mathbb{1}}^L\rangle$ at $\theta = 0$, the system evolves into the ground state $|\Psi_s^L\rangle$ by adiabatically threading a $\theta = 2\pi$ flux. Further increasing flux up to 4π will drive the system back to the identity ground state $|\Psi_{\mathbb{1}}^L\rangle$. (b) Charge transfer from one edge to the other edge on the cylinder geometry.

3. Modular Matrix

We further demonstrate the fractional quasiparticles in the bulk satisfy the so-called "semionic" statistics, as expected for Laughlin $\nu = 1/2$ state. In the topological quantum field theory, quasiparticle statistics is encoded in the modular matrices which describe the action of modular transformation on the topological groundstates[48–50]. The $\mathcal{S}-$matrix contains the mutual statistics information of the anyonic quasiparticles, such as quantum dimensions and fusion rules between different quasiparticles. The $\mathcal{U}-$matrix encodes the self-statistics of the quasiparticles, i.e. topological spin h_i. Here we utilize the route of the "twist" overlap between the two topologically degenerating groundstates $|\Psi_{\mathbb{1}}^L\rangle$ and $|\Psi_s^L\rangle$ to construct the modular $\mathcal{S}$ and $\mathcal{U}$ matrices[51–53].

The obtained results at $V_1 = 0.5, V_2 = V_3 = 1.0$ on $L_y = 4$ cylinder are

$$\mathcal{S} \approx \frac{1}{\sqrt{2}} \begin{bmatrix} 1 & 1 \\ 1 & -1 \end{bmatrix} + \begin{bmatrix} 0.029 & 0.053 \\ 0.005 & 0.036 + 0.033i \end{bmatrix}$$

$$\mathcal{U} \approx e^{-i\frac{3\pi}{4}} \begin{bmatrix} 1 & 0 \\ 0 & i \end{bmatrix} \times \begin{bmatrix} 1 & 0 \\ 0 & e^{i0.03\pi} \end{bmatrix}.$$

Indeed, the numerical obtained modular matrices are very close to the analytical prediction from $SU(2)_1$ Chern-Simons theory[48–50,69]: $\mathcal{S}^{SU(2)_1} = \frac{1}{\sqrt{2}} \begin{bmatrix} 1 & 1 \\ 1 & -1 \end{bmatrix}$ and $\mathcal{U}^{SU(2)_1} = e^{-i\frac{\pi}{12}} \begin{bmatrix} 1 & 0 \\ 0 & i \end{bmatrix}$. From $\mathcal{S}-$ and $\mathcal{U}-$ matrices, we obtain full statistics of fractionalized quasiparticles: 1) There are two kinds of quasiparticles in total: Identity $\mathbb{1}$ and semion s, and the total quantum dimension is $\mathcal{D} = \sqrt{2}$; 2) The fusion rule of quasiparticles (that specifies how the quasiparticles combine and fuse)[49]: $\mathbb{1} \times s = s$, $s \times s = \mathbb{1}$; 3) $\mathbb{1}$ and s respectively has topological spin (the phase factor for the quasiparticle obtained during a self-rotation of 2π): $h_{\mathbb{1}} = 0$, $h_s = 1/4$. These braiding statistics provides the strongest confirmation that the topological groundstate is equivalent to the bosonic FQH $\nu = 1/2$ state.

III. DISCUSSION AND CONCLUSION

We have established a phase diagram for the Bose-Hubbard model for kagome system at 1/3 filling number with the emergent FQH phase in the intermediate regime. We also address the nature of the quantum phase transitions between the FQH phase and solid phases (see Appendix D). We utilize several quantities, such as entanglement entropy, correlation length and groundstate wavefunction fidelity. The numerical evidences signal the first order character of the phase transition between FQH phase and the strip phase as well as the charge density wave state. Moreover, we also find that in all three phases, the obtained correlation length is much smaller than the cylinder width L_y, which confirms that our DMRG calculation offers a reliable phase diagram for the thermodynamic limit.

Regarding the laboratory realization for the emergent FQH state, a natural experimental setting for Bose-Hubbard physics is ultracold atomic gases[54]. One advantage of our model is that it only contains real nearest-neighbor hoppings and density-density interactions. Moreover, we also note that there are several existing candidates of spin$-1/2$ materials with kagome structure, such as $BaCu_3V_2O_8(OH)_2$[59], $Cu_3(Mg, Zn)O_7(OH)_2 \cdot H_2O$[60], $Cu_3V_2O_7(OH)_2 \cdot H_2O$[61], $Rb_2Cu_3SnF_{12}$[62] and $Dy_3Ru_4Al_{12}$[63], and each of them has its own interactions deserving to be studies more carefully under magnetic field for possible detecting of the exotic magnetization plateaus. But the fine tuning of second and third nearest neighbor interactions in such materials may be difficult to achieve. So the material-realization of our proposed FQH phase in condensed matter setting may depend on synthesising more kagome materials in the future.

In conclusion, we have presented a global phase diagram of an extended Bose-Hubbard model on the kagome lattice at fractional one-third filling. Importantly, the interplay between the underlying lattice and strong interaction gives birth to a fractional quantum Hall (FQH) liquid phase, even though the non-interacting band structure is topological trivial. We also provide complete characterization of the universal properties of the FQH phase, including ground state degeneracy, topological entanglement spectrum, fractionally quantized Chern number and anyonic quasiparticle statistics. To our best knowledge, this is the first example of a TRS breaking topological phase at one-third filling on kagome lattice system.

We believe our current work will inspire upcoming research efforts both in theoretical and experimental fields. From the theoretical side, the origin of topological phase in bosonic system is under intense study. Very recently, Ref.[70] proposed a plausible theory to understand the microscopic origin of chiral spin liquid on kagome lattice. However, this theory only applies to half filling on kagome system (At one-third filling, the mapping shown in that paper only gives topological trivial phase). Our current findings and also previous theoretical works[36,37] will stimulate further study on the origin of bosonic topological phases (or chiral spin liquid) on kagome lattice. Moreover, the present calculations show that the model of strongly interacting hard-core bosons can harbor rich and in-

teresting phases through interaction engineering. It is also interesting to study the interacting particles to be spinless or spinful fermions, since the possible topological liquid phase in fermionic models has been sought for a long time[10,11]. From the experimental side, our work will provide direction and insight in searching for the topological liquid phase in realistic materials with kagome lattice structure, or by engineering such systems in ultracold atomic settings. Thus our present findings would provide both theorists and experimentalists a rich playground in searching of new topological phases induced by strong interaction.

Appendix A: Method

In this paper, the calculations are based on the density-matrix renormralization group (DMRG) algorithm on cylinder geometry[64,65] and the exact diagonalization (ED) on torus geometry, both of which have been proven to be effective and complementary tools for studying realistic models containing arbitrary strong and frustrated interactions. On one hand, ED is straightforward in identifying the groundstate degeneracy on compactified spaces. But the drawback is that with the exponential growing of the Hilbert space, the accessible systems are limited to smaller sizes, up to $N_s = 36$ for this study. On the other hand, DMRG calculation allows us to obtain accurate groundstates and related entanglement measurements on much larger system sizes beyond the ED limit. Moreover, DMRG calculation also has the advantages of probing ground states with spontaneous symmetry breaking and topological ordering. The DMRG calculations on long cylinder tend to automatically select the groundstates with minimal entropy[66], which is helpful to study the fractionalized quasiparticle statistics in topological ordered states[52].

1. Details of DMRG Calculation

We study the cylinder system with open boundaries in the x direction and periodic boundary condition in the y direction. The available system sizes are cylinders of circumference $L_y = 3, 4, 5, 6$ (in unit of unit cell). For the largest system width ($L_y = 6$), we keep up to $M = 8400 \, U(1)$ states and reach the DMRG truncation error 5×10^{-7}.

The entanglement entropy and spectrum can be easily obtained in the DMRG. By partitioning the system into subsystems A and B, the groundstate wavefunction $|\psi\rangle$ can be decomposed according to Schmidt decomposition $|\psi\rangle =$

$\sum_i \lambda_i^{1/2} |\psi_A^i\rangle |\psi_B^i\rangle$, where λ_i are eigenvalues of the reduced density matrix $\hat\rho_A$ of subsystem A. Thus the entanglement entropy can be defined as $S_A = -tr[\hat\rho_A \ln \hat\rho_A] = -\sum_i \lambda_i \ln \lambda_i$. The eigenvalues $log\{\lambda_i\}$ plotted against the relative momentum quantum number Δk_y of the subsystem A, is defined as the entanglement spectrum[38].

2. Adiabatic DMRG and Fractionally Quantized Chern Number

We have used the numerical flux insertion experiment based on the adiabatical DMRG simulation to detect the topological Chern number of the bulk system[24,40,41]. To simulate the flux θ threading in the hole of a cylinder, we impose the twist boundary conditions along the y direction with replacing terms $b_{\mathbf{r}'}^\dagger b_{\mathbf{r}} + h.c. \rightarrow e^{i\theta_{\mathbf{r}'\mathbf{r}}} b_{\mathbf{r}'}^\dagger b_{\mathbf{r}} + h.c.$ for all neighboring $(\mathbf{r}, \mathbf{r}')$ bonds with hoppings crossing the y-boundary in the Hamiltonian (Eq. 1). The charge pumping from one edge to the other edge can be computed from $\langle \Delta Q(\theta) \rangle = Tr[\hat\rho_L(\theta)\hat{Q}(\theta)]$, where $\hat{Q}(\theta)$ is the $U(1)$ quantum number and $\hat\rho_L(\theta)$ is reduced density matrix of left half system. Due to the quantized Hall response, the Chern number of ground state is equal to the charge pumping by threading a $\theta = 2\pi$ flux[43]. To realize the adiabatic flux insertion, we use the step of flux insertion as $\Delta\theta = 0.25\pi$.

Appendix B: Classical Phase Diagram

In this section, we discuss the phase diagram of the model without hopping term $t = 0$, where the system reduces to a classical Ising model with competing antiferromagnetic interactions[17]. We compare the energy of four states, i.e., the $q = (0,0)$ state, the $q = (0,\pi)$ state, the stripe state, and the $\sqrt{3} \times \sqrt{3}$ state. The pattern of these states are shown in the inset of Fig. 6(a). Interestingly, we find that when both V_2, V_3 are larger than V_1, the stripe state always has the lowest energy; otherwise, the $q = (0,0)$ and $q = (0,\pi)$ states compete depending on the strengths of V_2 and V_3 (see Fig. 6(a)).
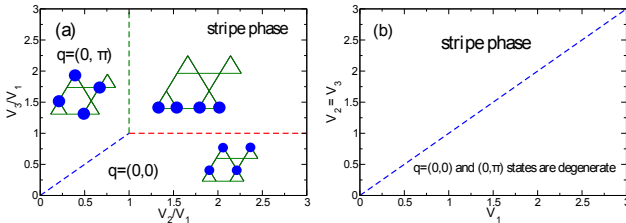
FIG. 6: Classical phase diagram in $\{V_1, V_2, V_3\}$ parameter space. (a)The phase diagram plotted in V_2/V_1 and V_3/V_1 parameter space. The insets show the unit cells of the different phases, where the large and small circles denote the occupied and the unoccupied sites. (b)The phase diagram plotted in V_1 and $V_2 = V_3$ parameter space.

It is interesting to compare this classical phase diagram with the quantum phase diagram as shown in Fig. 1(a). To compare them, we set $V_2 = V_3$ as shown in Fig. 6(b), where the system shows two phase regions, a stripe phase and a charge density wave phase region with the boundary at $V_2 = V_3 = V_1$. Interestingly, the charge density wave states with $q = (0,0)$ and $q = (0,\pi)$ are degenerated in the case of $V_1 < V_2$. In the quantum case, the degeneracy is lifted with the $q = (0,0)$ state having the lower energy. The FQH phase obtained by DMRG appears in the transition region between the stripe phase and the $q = (0,0)$ phase of the classical phase diagram. The emergence of the topological phase appears seems to arise as a result that quantum fluctuations destroy long-ranged orders around the transition region. This could serve as a guiding principle for finding topological phases in other models and/or on other lattices.
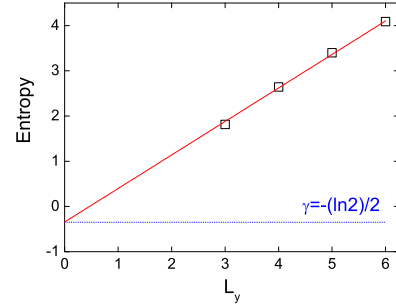
FIG. 7: Entanglement entropy scaling with L_y.

Appendix C: Topological entanglement entropy

For a gapped quantum phase with topological order, the topological entanglement entropy (TEE) γ is proposed to characterize the non-local entanglement[67,68]. Generally speaking, entropy has the form $S = \alpha L_y - \gamma$, where L_y is the boundary of the subsystem, and α is a non-universal constant. While a positive γ is a correction to the area law of entanglement and reaches a universal value determined by total quantum dimension $\mathcal{D}$ of quasiparticle excitations as $\gamma = \ln \mathcal{D}$. For the $\nu = 1/2$ Laughlin state, the quantum dimension of each quasiparticle is 1 (see main text), leading to the total quantum dimension $\mathcal{D} = \sqrt{2}$ and thus the TEE $\gamma = \ln \mathcal{D} = \frac{1}{2}\ln 2$.

By using the DMRG simulations, we obtain the minimal entropy state[51,66] with spontaneously broken time-reversal symmetry and calculate the corresponding Von Neuman entanglement entropy. The converged entropy are available for $L_y = 3, 4, 5, 6$ cylinders. For $V_1 = 0.5, V_2 = 1.0, V_3 = 1.0$, we make a linear fitting of the entropy data for $L_y = 3, 4, 5, 6$ cylinders, and find the TEE $\gamma \approx 0.343 \pm 0.075$. (If we make the linear fitting based on data for $L_y = 4, 5, 6$ (not shown), the obtained result is $\gamma \approx 0.241 \pm 0.098$). Despite some uncertainty in the fitting, the obtained TEE approaches the prediction of the $\nu = 1/2$ Laughlin state $\gamma = \frac{1}{2}\ln 2 \approx 0.346$.
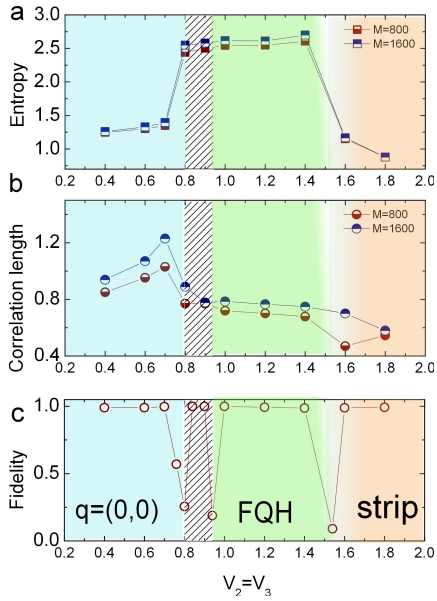
FIG. 8: (a) Entanglement entropy and (b) correlation length versus $V_2(= V_3)$ by setting $V_1 = 0.5$. The calculations are performed on $L_y = 4$ cylinder, by keeping $M = 800$ (brown dots) and 1600 (blue dots) states. (c) Wavefunction fidelity plotted as $V_2(= V_3)$ by setting $V_1 = 0.5$. The calculations are performed on $L_y = 4$ cylinder, by keeping $M = 800$.

Appendix D: Quantum phase transitions

In order to uncover the nature of corresponding phase transitions between FQH phase and solid phases, we inspect several quantities that are expected to be sensitive to a phase transition, such as the entanglement entropy S, and correlation length ξ. Both quantities are expected to show a finite jump when crossing a first order transition. We also calculate the groundstate wavefunction fidelity $F = |\langle\psi(V)|\psi(V + \delta V)\rangle|$ (V is some parameter in Hamiltonian)[65], which can faithfully describe the first-order transition or energy level crossing.

We show the results along the reference line in Fig. 1 (in the main text), by fixing $V_1 = 0.5$ and varying $V_2 = V_3$. In Fig. 8(a), it is found that the entanglement entropy shows a sharp jump around $V_2 = V_3 \approx 0.8$ and a drop around $V_2 = V_3 \approx 1.5$. We also observe the similar behavior when looking at the correlation length, as shown in Fig. 8(b). Both of these two measurements signals a direct first order phase transition between FQH phase and solid phases. In addition, we also find that, between the FQH phase and charge density wave $q = (0,0)$ phase, there exists a narrow window for the coexistence of both FQH nature and the charged order, as shown by the shaded area in the phase diagram. We have checked that, in this intermediate regime, the groundstate hosts the quantized Chern number $C = 1/2$, but develops weak charge order. From the wavefunction fidelity in Fig. 8(c), it is shown a first-order transition between the coexistence region and the FQH phase ($q = (0,0)$ phase).

Moreover, when studying the topological order on cylinder geometry with finite width L_y, the correlation length ξ of the ground state offers a natural consistency check for the assumption that the value of L_y is large enough to be representative of the thermodynamic limit. The correlation length is defined by $\xi = -\ln|\epsilon_1/\epsilon_2|$, where $\epsilon_{1,2}$ are two largest eigenvalue from transfer matrix[65]. If L_y is much larger than ξ, we indeed expect finite size effects to be very small. Indeed, in Fig. 8(b), the condition $L_y > \xi$ is satisfied so that our DMRG calculation offers a reliable and relevant results for thermodynamic limit. Based on these measurements, we expect the finite size effect should be small in our calculations.

[1] D. C. Tsui, H. L. Stormer, and A. C. Gossard, Phys. Rev. Lett. **48**, 1559 (1982).

[2] R. B. Laughlin, Phys. Rev. Lett. **50**, 1395 (1983).

[3] T. Neupert, L. Santos, C. Chamon, and C. Mudry, Phys. Rev. Lett. **106**, 236804 (2011).

[4] E. Tang, J.-W. Mei, and X.-G. Wen, Phys. Rev. Lett. **106**, 236802 (2011).

[5] K. Sun, Z. Gu, H. Katsura, and S. Das Sarma, Phys. Rev. Lett. **106**, 236803 (2011).

[6] D. Sheng, Z.-C. Gu, K. Sun, and L. Sheng, Nat Commun **2**, 389 (2011).

[7] N. Regnault and B. A. Bernevig, Phys. Rev. X **1**, 021014 (2011).

[8] X. G. Wen, F. Wilczek, and A. Zee, Phys. Rev. B **39**, 11413 (1989).

[9] X. G. Wen, Phys. Rev. B **44**, 2664 (1991).

[10] S. Raghu, X.-L. Qi, C. Honerkamp, and S.-C. Zhang, Phys. Rev. Lett. **100**, 156401 (2008).

[11] J. Wen, A. Rüegg, C.-C. J. Wang, and G. A. Fiete, Phys. Rev. B **82**, 075125 (2010).

[12] K. Sun, H. Yao, E. Fradkin, and S. A. Kivelson, Phys. Rev. Lett. **103**, 046811 (2009).

[13] Y. Zhang, Y. Ran, and A. Vishwanath, Phys. Rev. B **79**, 245331 (2009).

[14] W.-F. Tsai, C. Fang, H. Yao, and J.-P. Hu, New J. Phys. **17**, 055016 (2015).

[15] M. Di Liberto, A. Hemmerich, C. Morais Smith, arXiv.1604.06055v1.

[16] J. Motruk, A. G. Grushin, F. de Juan, and F. Pollmann, Phys. Rev. B 92, 085147 (2015).

[17] S. Capponi and A. M. Läuchli, Phys. Rev. B 92, 085146 (2015).

[18] K. Ferhat and A. Ralko, Phys. Rev. B **89**, 155141 (2014).

[19] F. Pollmann, K. Roychowdhury, C. Hotta, and K. Penc, Phys. Rev. B **90**, 035118 (2014).

[20] S. Nishimoto, M. Nakamura, A. O'Brien, and P. Fulde, Phys. Rev. Lett. **104**, 196401 (2010).

[21] S.-S. Gong, W. Zhu, D. N. Sheng, O. I. Motrunich, and M. P. A. Fisher, Phys. Rev. Lett. **113**, 027201 (2014).

[22] P. W. Anderson, Mater. Res. Bull. **8**, 153 (1973).

[23] V. Kalmeyer and R. B. Laughlin, Phys. Rev. Lett. **59**, 2095 (1987).

[24] S. S. Gong, W. Zhu, and D. N. Sheng, Sci. Rep. **4**, 06317 (2014).

[25] Y.-C. He, D. N. Sheng, and Y. Chen, Phys. Rev. Lett. **112**, 137202 (2014).

[26] B. Bauer, L. Cincio, B. Keller, M. Dolfi, G. Vidal, S. Trebst, and A. Ludwig, Nat Commun **5**, 6137 (2014).

[27] S.-S. Gong, W. Zhu, L. Balents, and D. N. Sheng, Phys. Rev. B **91**, 075112 (2015).

[28] A. Wietek, A. Sterdyniak, and A. M. Läuchli, Phys. Rev. B **92**, 125122 (2015) .

[29] L. Messio, B. Bernu, and C. Lhuillier, Phys. Rev. Lett. **108**, 207204 (2012).

[30] S. V. Isakov, S. Wessel, R. G. Melko, K. Sengupta, and Y. B. Kim, Phys. Rev. Lett. **97**, 147202 (2006).

[31] S. Nishimoto, N. Shibata, and C. Hotta, Nat Commun **4**, 2278 (2013).

[32] S. Capponi, O. Derzhko, A. Honecker, A. M. Läuchli, and J. Richter, Phys. Rev. B **88**, 144416 (2013).

[33] S. A. Parameswaran, I. Kimchi, A. M. Turner, D. M. Stamper-Kurn, and A. Vishwanath, Phys. Rev. Lett. **110**, 125301 (2013).

[34] K. Roychowdhury, S. Bhattacharjee, and F. Pollmann, ArXiv e-prints (2015), 1505.05998.

[35] X. Plat, F. Alet, S. Capponi, and K. Totsuka, ArXiv e-prints (2015), 1505.07943.

[36] K. Kumar, K. Sun, and E. Fradkin, Phys. Rev. B **90**, 174409 (2014).

[37] K. Kumar, K. Sun, and E. Fradkin, Phys. Rev. B 92, 094433 (2015).

[38] H. Li and F. D. M. Haldane, Phys. Rev. Lett. **101**, 010504 (2008).

[39] X. G. Wen, Phys. Rev. B **41**, 12838 (1990).

[40] W. Zhu, S. S. Gong, and D. N. Sheng, J. Stat. Mech. p. P08012 (2014).

[41] M. P. Zaletel, R. Mong, and F. Pollmann, J. Stat. Mech. p. P10007 (2014).

[42] Y.-C. He, D. N. Sheng, and Y. Chen, Phys. Rev. B **89**, 075110 (2014).

[43] R. B. Laughlin, Phys. Rev. B **23**, 5632 (1981).

[44] M. Oshikawa, Phys. Rev. Lett. **84**, 1535 (2000).

[45] D. N. Sheng, X. Wan, E. H. Rezayi, K. Yang, R. N. Bhatt, and F. D. M. Haldane, Phys. Rev. Lett. **90**, 256802 (2003).

[46] Y.-F. Wang, Z.-C. Gu, C.-D. Gong, and D. N. Sheng, Phys. Rev. Lett. **107**, 146803 (2011).

[47] S. H. Simon, F. Harper, and N. Read, ArXiv e-prints (2015), 1506.08197.

[48] X. G. Wen, Int. J. Mod. Phys. B **04**, 239 (1990).

[49] P. Francesco, P. Mathieu, and D. Snchal, *Conformal Field Theory* (1997).

[50] S. Dong, E. Fradkin, L. R. G., and S. Nowling, JHEP **05**, 016 (2008).

[51] Y. Zhang, T. Grover, A. Turner, M. Oshikawa, and A. Vishwanath, Phys. Rev. B **85**, 235151 (2012).

[52] L. Cincio and G. Vidal, Phys. Rev. Lett. **110**, 067208 (2013).

[53] W. Zhu, D. N. Sheng, and F. D. M. Haldane, Phys. Rev. B **88**, 035122 (2013).

[54] I. Bloch, J. Dalibard, and W. Zwerger, Rev. Mod. Phys. **80**, 885 (2008).

[55] G.-B. Jo, J. Guzman, C. K. Thomas, P. Hosur, A. Vishwanath, and D. M. Stamper-Kurn, Phys. Rev. Lett. **108**, 045305 (2012).

[56] H. P. Büchler, E. Demler, M. Lukin, A. Micheli, N. Prokof'ev, G. Pupillo, and P. Zoller, Phys. Rev. Lett. **98**, 060404 (2007).

[57] S. Flling, F. Gerbier, A. Widera, O. Mandel, T. Gericke, and I. Bloch, Nature **434**, 481 (2005).

[58] G. Jotzu, M. Messer, R. Desbuquois, M. Lebrat, T. Uehlinger, D. Greif, and T. Esslinger, Nature **515**, 237 (2014).

[59] H. Okamoto, Y.and Yoshida and Z. Hiroi, J. Phys. Soc. Jpn. **78**, 033701 (2009).

[60] O. Janson, J. Richter, and H. Rosner, Phys. Rev. Lett. **101**, 106403 (2008).

[61] H. Ishikawa, M. Yoshida, K. Nawa, M. Jeong, S. Krämer, M. Horvati, C. Berthier, M. Takigawa, M. Akaki, A. Miyake, et al., Phys. Rev. Lett. **114**, 227202 (2015).

[62] T. F. Y. Matan, K.and Ono, T. J. Sato, J. Yamaura, M. Yano, and K. H. T. H. Morita, Nat Phys **6**, 865 (2010).

[63] D. I. Gorbunov, M. S. Henriques, A. V. Andreev, A. Gukasov, V. Petříček, N. V. Baranov, Y. Skourski, V. Eigner, M. Paukov, J. Prokleška, et al., Phys. Rev. B **90**, 094405 (2014).

[64] S. R. White, Phys. Rev. Lett. **69**, 2863 (1992).

[65] I. P. McCulloch, ArXiv e-prints (2008), 0804.2509.

[66] H. C. Jiang, Z. Wang, and L. Balents, Nat Phys **8**, 902 (2012).

[67] A. Kitaev and J. Preskill, Phys. Rev. Lett. **96**, 110404 (2006).

[68] M. Levin and X.-G. Wen, Phys. Rev. Lett. **96**, 110405 (2006).

[69] The predicted prefactor of $SU(2)_1$ CFT is $e^{-ic\frac{2\pi}{24}} = e^{-i\frac{\pi}{12}}$, where $c = 1$ is central charge. Taking into account the fact that definition of central charge is module 8[49], the obtained result $c \approx 9\%8 = 1$ is equivalent to the expectation $c = 1$ ($e^{-i3\pi/4} = e^{-i9\pi/12}$).

[70] Y. C. He, S. Bhattacharjee, F. Pollmann and R. Moessner, Phys. Rev. Lett. 115, 267209 (2015).